

# Static Friction of Liquid Marbles

Yui Takai,<sup>1,\*</sup> Kei Mukoyama,<sup>1,\*</sup> Pritam Kumar Roy,<sup>1</sup> Guillaume Lagubeau,<sup>2</sup> David Quéré,<sup>3</sup> Samuel Poincloux,<sup>4,†</sup> and Timothée Moutherde<sup>1,‡</sup>

<sup>1</sup>*The University of Tokyo, Department of Mechanical Engineering, Tokyo, Japan.*

<sup>2</sup>*Université de Lille, CNRS, UMR 8520-IEMN, Lille, France.*

<sup>3</sup>*ESPCI Paris, Physique et Mécanique des Milieux Hétérogènes, UMR 7636 du CNRS, Paris, France.*

<sup>4</sup>*Department of Physical Sciences, Aoyama Gakuin University, Sagami, Japan.*

Liquid marbles, droplets coated with a granular layer, are highly mobile as particles prevent capillary adhesion with the substrate. Yet, they exhibit static friction due to their granular shell, which resists rolling until it yields. This friction depends on the shell geometry and increases exponentially with grain density, indicating a logistic dependence of interparticle compressive forces on surface coverage, confirmed by yielding measurements in granular rafts. These results reveal the shell's dual role, and establish liquid marbles as a model system for probing granular raft mechanics.

Manipulating small volumes of liquid is challenging owing to capillary forces that pin droplets below the millimeter scale. A common approach to prevent capillary pinning is to form non-wetting states by separating the liquid from the solid via a gas layer. The gas layer can be formed actively by air entrainment from a fast-moving surface [1, 2] or, in the Leidenfrost effect, by an evaporative vapor layer [3]. On superhydrophobic surfaces, air is stabilized passively by hydrophobic micro/nano structures [4, 5]. Alternatively, structures can be embedded at the liquid surface by coating the droplet with particles, forming so-called liquid marbles [6], whose non-wetting state is independent of the substrate. In addition, the particles' properties can be tailored to bring additional functionalities to droplets, for example, allowing manipulation through external stimuli, including light [7] and magnetic fields [8], or allowing the handling of hot liquids [9]. This versatility makes liquid marbles powerful tools for applications including microreactors in chemistry [10] and biology [11, 12], soft robotics [13], sensing [14], or materials design [15].

Both liquid marbles and droplets on superhydrophobic surfaces exhibit very low apparent static friction, and even a slight slope can initiate their motion. For droplets, this static friction arises from contact angle hysteresis and capillary forces [16, 17]. In contrast, the static friction of liquid marbles appears to resemble solid-solid friction [18] for moderate volumes (from 10 to 50  $\mu\text{L}$ ). However, the underlying physical mechanisms responsible for this behavior remain largely unexplored. This paper explores how liquid marble static friction results from the coupling between asphericity-induced deformation under rolling and the granular raft encapsulating the droplet.

We prepare liquid marbles by coating water drops — surface tension  $\gamma = 72 \text{ mN/m}$ , density  $\rho = 1000 \text{ kg/m}^3$  and volume  $\Omega$  (Fig. 1a) — with lycopodium particles of typical diameter  $d = 30 \mu\text{m}$  (Fig. 1b), that cover a surface fraction  $\phi$  of the liquid interface. This preparation method ensures a constant initial particle's surface fraction,  $\phi_o \approx 0.83 \pm 0.01$  (see End Matter for details on mar-

ble preparation and experimental determination of  $\phi_o$ ). The particles at the interface reduce the effective surface tension  $\gamma_{\text{eff}}(\phi)$  [19, 20], and its value for  $\phi_o$  can be obtained from the marble's shape  $\gamma_{\text{eff}}(\phi_o) \approx 53 \pm 1 \text{ mN/m}$ . The marbles are then deposited on a horizontal silicon wafer, which is gradually tilted until reaching the angle  $\alpha$ , at which the marbles start moving (Fig. 1a). The departing angle  $\alpha$ , measured using a digital goniometer (Monotaro, Japan), corresponds to the slope for which the weight projected along the substrate  $F = \rho\Omega g \sin \alpha \approx \rho\Omega g \alpha$  overcomes the effective static friction force, with  $g$  the acceleration of gravity. Here, we neglect the contribution of the lycopodium's mass that corresponds to less than 3% of the total mass.

We first investigate how the shape of liquid marbles influences their departing angle. To this end, we vary the initial volume  $\Omega$  from 1.5  $\mu\text{L}$  to 300  $\mu\text{L}$ , and report the corresponding effective static friction force  $F$  in Fig. 1c. The experiments reveal three key observations. (i) The marbles start moving with a rolling motion (see Supplemental Video 1), therefore,  $F$  corresponds to a static rolling friction. (ii) The static friction increases with volume, but at a slower rate than the linear scaling predicted by Amontons-Coulomb sliding friction, which would imply a departure angle independent of the particle weight [18]. (iii) The dependence of  $F$  on volume exhibits two regimes: a slow increase when  $\Omega$  is smaller than  $\sim 10 \mu\text{L}$ , followed by faster rise for droplets above  $\sim 10 \mu\text{L}$ . The shape of liquid marbles depends on their volume. Denoting the capillary length as  $a(\phi) = \sqrt{\gamma_{\text{eff}}(\phi)/\rho g}$ , marbles with volumes smaller than  $a^3$  remain nearly spherical (Fig. 2a), while larger ones are increasingly flattened by gravity, resulting in a higher surface-to-volume ratio (Fig. 2b). For  $\phi = \phi_o$ , we find  $a^3(\phi_o) \approx 12 \mu\text{L}$ , consistent with the observed transition volume. This suggests that the marble shape may govern the transition between the two friction regimes observed for  $F$ .

Based on these observations, we assume that the static friction of liquid marbles originates from the resistance of the granular shell to rolling, which we now seek to model.

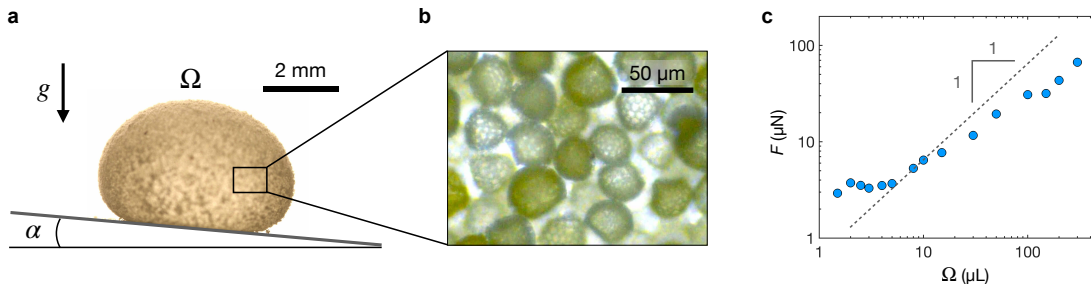


Figure 1. (a) A water marble with volume  $\Omega$  is deposited on a silicon wafer. The substrate is slowly tilted from the horizontal until the marble departs at an angle  $\alpha$ . The liquid marble on the photo has a volume  $\Omega = 50 \mu\text{L}$ . (b) Microscope image of the hydrophobic lycopodium particles with a typical diameter of  $30 \mu\text{m}$  used to form the granular shell of the marbles. (c) Liquid marbles static friction  $F$  plotted as a function of their volume  $\Omega$  on log-log scales. The dashed line with slope one corresponds to the Amontons–Coulomb sliding friction between the marble and the substrate.

Liquid marbles—even those smaller than the capillary length—are never perfectly spherical owing to gravity. As a result, rolling without sliding induces deformation of their shells. Upon rolling, the flattened patch in contact with the substrate travels, shearing the granular shell in the process. The transition from static to rolling marbles is thus governed by the in-plane shear deformation of the granular shell, which we assimilate to a granular raft [21, 22] wrapped around the liquid. We adopt an energy-based approach to determine the departing angle  $\alpha$ . The marble rolls down the incline by a small distance  $\delta x$  when the gravitational energy gain  $\delta E_g \approx \rho g \Omega \alpha \delta x$  overcomes the energy  $\delta E_d$  dissipated by shearing the granular shell. We note that the viscous dissipation in the liquid is negligible since we are looking at the onset of rolling under quasi-static tilting of the substrate. We then assume that rolling by  $\delta x$  imposes a homogeneous shear strain  $\delta \epsilon$  to a surface area  $S$  of the granular shell (see Fig. 2a and b). The energy dissipated in this shell portion of volume  $Sd$ , then writes  $\delta E_d \sim Sdq_y \delta \epsilon$ , with  $q_y$  the yield stress of the granular shell [23]. This estimation neglects the elastic response of the granular assembly, assuming that all imposed shear is dissipated rather than stored elastically. We adopt a cohesionless Mohr–Coulomb criterion for the yield stress,  $q_y = \mu p(\phi)$ , with  $\mu$  a macroscopic friction coefficient [24] and  $p(\phi)$  the average normal stress within the granular shell, which depends on the grain surface fraction  $\phi$ . This stress reduces the effective surface tension of the marble, such that  $\gamma_{\text{eff}} = \gamma - p(\phi)d$  [21, 25]. We rewrite the pressure term as  $p(\phi) = \gamma f(\phi)/d$ , introducing a dimensionless function  $f(\phi)$  that captures the dependence on the surface fraction. The effective surface tension then becomes  $\gamma_{\text{eff}} = \gamma(1 - f(\phi))$ , so that  $f$  also quantifies how  $\gamma_{\text{eff}}$  varies with  $\phi$ . Substituting this into the energy balance  $\delta E_g \sim \delta E_d$ , we obtain the departing angle  $\alpha$ :

$$\alpha \approx \frac{Sa^2}{\Omega} \frac{\delta \epsilon}{\delta x} \mu \frac{f(\phi)}{1 - f(\phi)} \quad (1)$$

The sheared shell surface  $S$  and the shear strain  $\delta \epsilon$  involved in dissipation are primarily controlled by the aspheric deformation of the marble, analogous to shear in non-wetting rolling droplets [26]. Gravity flattens the marbles, producing a contact disk of diameter  $l$  on the substrate and setting the sheared region height. We distinguish two cases based on the marble geometry: (i) Large marbles are flattened by gravity to a height of approximately  $2a$ . Assuming a cylindrical shape with base diameter  $l$ , their volume is given by  $\Omega \approx \pi l^2 a/2$ . Due to the large deformations of these marbles, we assume that the entire surface  $S \approx \pi l^2/2 + 2\pi l a$  is sheared over the marbles’ height  $2a$ , hence  $\delta \epsilon \approx \delta x/2a$  (Fig. 2b). (ii) Small marbles are quasi-spherical with radius  $R$  and volume  $\Omega \approx 4\pi R^3/3$ . The contact region is obtained by balancing the weight  $\rho g R^3$  with the Laplace pressure integrated over the contact area,  $\gamma_{\text{eff}} l^2/R$ , yielding  $l \sim R^2/a$  [26]. Most of the spherical marble rotates as a rigid body, and thus shear is confined near the contact and extends over a distance  $l$  (Fig. 2a). Hence, we have  $S \approx 2\pi R l$  and  $\delta \epsilon \approx \delta x/l$ . Combining Eq. 1 with the expressions for  $S$  and  $\delta \epsilon$  in the two limit cases, we obtain for small marbles:

$$\alpha \approx (6\pi^2)^{1/3} \left( \frac{a^3}{\Omega} \right)^{2/3} \mu \frac{f(\phi)}{(1 - f(\phi))^2} \quad (2)$$

and for the large ones:

$$\alpha \approx \frac{1}{2} \left( 1 + \sqrt{\frac{8\pi a^3}{\Omega}} \right) \mu \frac{f(\phi)}{1 - f(\phi)}, \quad (3)$$

Our model predicts three successive regimes for  $\alpha$  as the volume  $\Omega$  increases. For small volumes,  $\alpha$  scales as  $\Omega^{-2/3}$ , followed by a transition regime with  $\Omega^{-1/2}$ , before reaching a plateau at large volumes. Although the dissipation mechanisms differ, the two first scalings are also observed for drops, whereas the constant regime appears to be specific to liquid marbles.

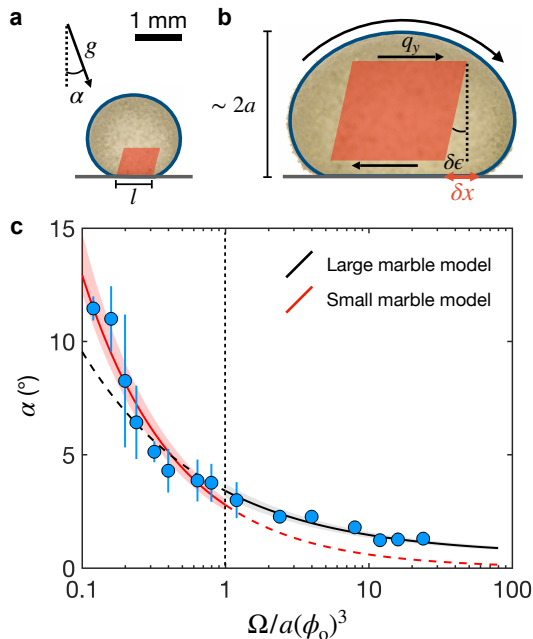


Figure 2. (a-b). Sketch of liquid marbles rolling on a surface tilted by  $\alpha$ , the red area represents the sheared part of the marbles for a liquid marble smaller (a) or larger (b) than the capillary length. (c) Departing angle  $\alpha$  as a function of the liquid marble normalized volume  $\Omega/a(\phi_o)^3$  in lin-log scale. The black line represents Eq. 3 with  $f(\phi_o) = 0.26$ ,  $a(\phi_o) = 2.3$  mm and  $\mu = 0.055 \pm 0.005$  and the red line shows Eq. 2 adjusted by a factor of 0.46. The plain lines indicate the region on which the data is fitted, and the 95% interval of confidence of the fits is indicated with colored areas.

To compare our model with experiments, we estimate the friction coefficient  $\mu$  by fitting Eq. 3 in the large volume regimes,  $\Omega/a^3 > 1$ , where  $\Omega$  only slightly affects  $\alpha$ . Taking  $f(\phi_o) = 0.26$  and  $a(\phi_o) \approx 2.3$  mm, which correspond to  $\gamma_{\text{eff}}(\phi_o) \approx 53$  mN/m, the experimental data is best adjusted with  $\mu = 0.055 \pm 0.005$  (shown as a black line in Fig. 2c). Using this value for the friction coefficient, the data for small volumes is well predicted by adjusting Eq. 2 with a coefficient 0.46 (shown as a red line in Fig. 2c), a value close to unity which accounts for the geometry-dependent approximations. The low value of the friction coefficient reflects that granular rafts at  $\phi_o$  are fragile assemblies, yielding easily under shear. Even though the departing angle  $\alpha$  remains low across all tested volumes, a signature of the high mobility of non-wetting states, our model captures its variations in the two regimes.

Our model also predicts that the static friction of liquid marbles depends on the normal force between grains, which increases with the particle surface fraction  $\phi$ , through the function  $f(\phi)$  [21, 25, 27]. We test this hypothesis with a second experiment. We prepare marbles with initial volume  $\Omega_o$ , surface area  $S_o$ , and surface fraction  $\phi_o$ . Then we vary the marble's surface area  $S$ ,

either by adding ( $\delta\Omega > 0$ ) or removing ( $\delta\Omega < 0$ ) water using a microsyringe (SGE Analytical Science). The surface change, at constant initial number of particles  $\phi_o S_o$ , leads to a new surface fraction  $\phi = (S_o/S)\phi_o$ . We show in Fig. 3a photographs of deflated and inflated 100  $\mu\text{L}$  liquid marbles. From these images, we measure the total surface area  $S$  using the Pappus-Guldinus theorem, assuming a symmetry of revolution (see End Matter for details). The surface fraction  $\phi$  is plotted in Fig. 3b as a function of the relative volume variation  $\delta\Omega/\Omega_o$  for liquid marbles with initial volumes  $\Omega_o = 50, 100$  and  $150$   $\mu\text{L}$ . For all volumes, the data decrease linearly with  $\delta\Omega/\Omega_o$  and are well fitted by  $\phi = \phi_o(1 - 0.58\delta\Omega/\Omega_o)$  (black line in Fig. 3b). We use this equation to estimate the surface fraction of all liquid marbles. Using the resulting modified marbles with volume  $\Omega$ , surface area  $S$ , and particle surface fraction  $\phi$ , we measure the departing angle  $\alpha$  as a function of  $\phi$  for marbles with initial volumes ranging from 50 to 150  $\mu\text{L}$ . The results are plotted in Fig. 3c. The graph reveals that  $\alpha$ , hence the marbles' static friction, varies exponentially with the surface fraction  $\phi$  (see Supplemental Video 2). The departing angle, which corresponds to the friction-to-weight ratio, abruptly increases from less than 0.8% for deflated marbles with  $\phi \sim 0.7$  to more than 50% for deflated marbles with  $\phi$  close to 1. This effect dominates over the weak variations due to the initial marble volume in the large marbles regime (Eq. 3). This observation also reveals that a non-wetting situation is not sufficient to ensure high mobility; a relatively low surface fraction is also a necessary condition. The exponential nature of the relationship is more clearly revealed in the inset, where the same data — normalized by  $\alpha_o$  (the sliding angle at  $\phi_o$ ) — are plotted against  $\phi$  on a semi-logarithmic (log-lin) scale, resulting in a linear trend well captured by an exponential fit of the form  $\alpha/\alpha_o = \exp[\beta(\phi - \phi_o)]$ , with  $\beta = 15.4 \pm 1.7$  (black line).

From this experimental result and using Eq. 3 in the asymptotic limit  $\Omega/a^3 \gg 1$ , we derive an analytical estimate for  $f(\phi)$ , which takes the form of a logistic function:

$$f(\phi) = \frac{1}{1 + e^{-\beta(\phi - \phi_c)}}, \quad (4)$$

with  $\phi_c = \phi_o - (1/\beta)\ln(\gamma/\gamma_{\text{eff}}(\phi_o) - 1)$ , that is  $\phi_c \approx 0.90 \pm 0.01$ . The model for  $f(\phi)$  thus implies that the effective surface tension  $\gamma_{\text{eff}}$  decreases following a logistic function of the particle surface fraction  $\phi$ , dropping from  $\gamma$  at low density to zero at high density, in agreement with the expected behavior of the surface tension of liquid marbles [25]. In contrast, the internal pressure  $p(\phi)$  in the granular shell increases with the logistic function  $f(\phi)$ . This suggests that the functional form we derive may capture generic features of densely packed particulate systems. We note that  $\phi_c$  is independent of the choice of  $\phi_o$ , despite its explicit appearance in the ex-

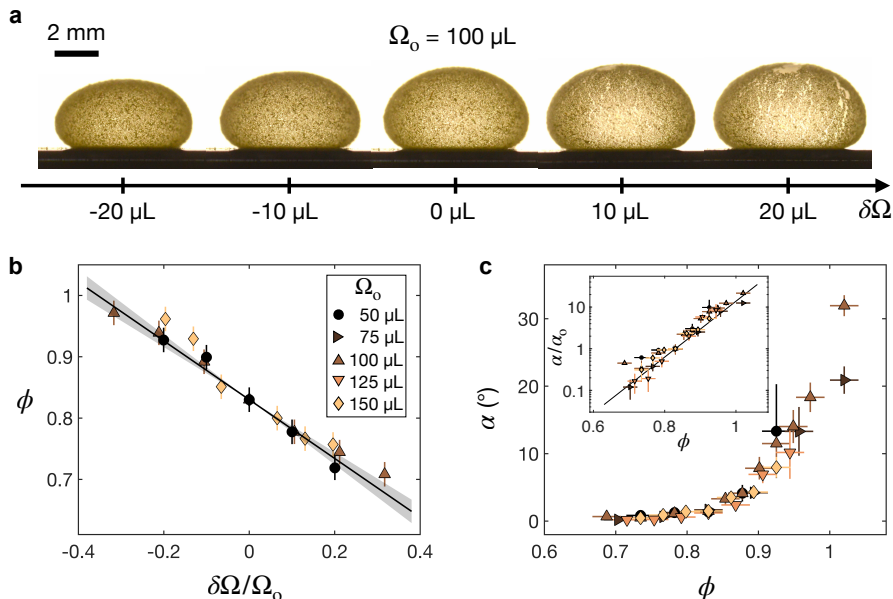


Figure 3. (a) Photographs of lycopodium liquid marbles with initial volume  $\Omega_0 = 100 \mu\text{L}$  to which a volume  $\delta\Omega$  of liquid is either removed ( $\delta\Omega < 0$ ) or added ( $\delta\Omega > 0$ ) while keeping constant the number of particles at the surface. We show  $\delta\Omega$  varying from  $-20 \mu\text{L}$  to  $20 \mu\text{L}$  and the central image corresponds to the standard liquid marble preparation. (b) Particle surface fraction  $\phi$  as a function of the volume relative variation  $\delta\Omega/\Omega_0$  for liquid marbles with initial volumes  $\Omega_0 = 50, 100$  and  $150 \mu\text{L}$ . The surface and volumes are measured by image analysis, assuming a symmetry of revolution. The black line represents the linear fit  $\phi = \phi_0(1 - 0.58\delta\Omega/\Omega_0)$ , with  $\phi_0 = 0.83$ . The shaded area represents the 95% confidence interval of the fit. (c) Departing angle  $\alpha$  as a function of the particle surface fraction  $\phi$  for marbles with initial volumes  $\Omega_0$  ranging from 50 to 150  $\mu\text{L}$ . Inset:  $\alpha$  normalized by  $\alpha_0$  (its value for  $\phi_0 = 0.83$ ) plotted as a function of  $\phi$  on a log-lin scale. The black line shows the best exponential fit of the data with  $\exp(\beta(\phi - \phi_0))$ , where  $\beta = 15.4 \pm 1.7$ .

pression.

To test the generality of our findings, we turn to two-dimensional granular rafts, where the effective confining pressure can be probed independently — for instance, by measuring the force needed to yield the raft via an obstacle-dragging experiment. To do this, we prepare a granular raft by depositing a mass  $m_g$  of glass beads, each with a diameter  $d = 110 \pm 20 \mu\text{m}$  and density  $\rho_g$ , onto the surface of a water bath contained within a Langmuir–Blodgett trough. The particles form a monolayer with surface coverage  $\phi$ , which is controlled by adjusting the liquid bath surface area  $S_t$ . The surface fraction is given by  $\phi = 3m_g/2\rho_g dS_t$ . To measure the interaction force between grains, we insert the core of a vertical glass optical fiber (length ranging from 3 to 5.5 cm depending on the experiment, and diameter 125  $\mu\text{m}$ ) into the raft. The fiber is clamped at one end, while the trough is translated horizontally at a velocity (1 mm/s) low enough to avoid dynamic effects. As the fiber encounters resistance from the granular monolayer, it bends, and the resulting force  $F_y$  is estimated from the deflection  $\delta$  (Fig. 4, inset), using Hooke’s law,  $F_y = k\delta$ , where  $k$  is the effective spring constant of the fiber. The value of  $k$  is determined from static deflection of the fiber under its own weight when clamped horizontally, yielding  $k$  from 10 mN/m to 60 mN/m for long and short fibers, respec-

tively. In the steady state, the fiber locally yields the granular raft, we therefore expect the exerted force to scale as  $F_y \sim q_y$ , hence  $F_y \sim f(\phi)$ , and by normalizing with the asymptotic force at large  $\phi$ :  $f(\phi) = F_y/F_y^{\text{max}}$ . Measuring  $F_y(\phi)$  thus provides an independent way to probe the functional form of  $f(\phi)$ , and consequently the effective surface tension of the interface.

In Fig. 4, we report the variation of  $f(\phi) = 1 - \gamma_{\text{eff}}/\gamma$  with  $\phi$  using three different estimations: the analytical prediction from Eq. 4 (black line); values obtained from the liquid marbles departing angles  $\alpha/\alpha_0$  using the Eq. 3 in the large volume limit (data color-coded from black to beige); and from the raft forces measurements  $f(\phi) = F_y/F_y^{\text{max}}$  (red data). The different estimations are in very good agreements with each others, spanning the full range of  $\gamma_{\text{eff}}/\gamma$  between 0 and 1. The agreement between marble- and raft-based measurements confirms that the static rolling friction of liquid marbles is governed by the yielding of their granular shell, which behaves as a two-dimensional raft. Moreover, the function  $f(\phi)$  appears independent of particle material and measurement method, suggesting that it reflects an intrinsic structural property of granular rafts. We thus search for geometrical interpretations for  $f(\phi)$  onset and saturation values. Remarkably, the yield starts to increase for  $\phi \sim 0.65$ , a value close to 0.676, the 2D

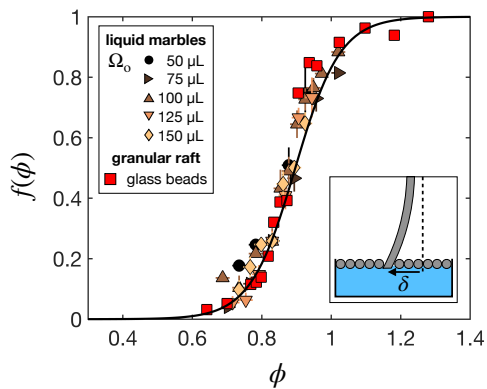


Figure 4.  $f(\phi)$  as a function of  $\phi$  obtained from: (i) Departing angles of inflated and deflated liquid marble’s with initial volume  $\Omega_0$  ranging from 50 to 150  $\mu\text{L}$  (color-coded from black to beige). Values are obtained using Eq. 3 in the asymptotic large-volume regime. (ii) Force measurements in a 2D granular raft (red data). The black line represents the logistic function of Eq. 4. Inset: Schematic of the experimental setup used to measure yield in granular rafts. The force is obtained from the deflection  $\delta$  of a calibrated fiber.

percolation threshold for monodisperse disks [28]. From this point, all particles are connected, so that adding particles increases the contacts in all the raft leading to an exponential increase of the pressure. The logistic function then reaches its inflection point for a density  $\phi \sim 0.90$ , a value that nicely matches the close packing limit for 2D disks  $\pi/\sqrt{12} \approx 0.907$  [29]. This observation allows us to rationalize the saturation: above this close-packed regime, the interface starts to deform — as observed with rafts [22, 30–32] and liquid marbles [25] — so that added particles generate forces that are no longer confined in-plane, hence the saturation. This also explains why the surface fraction  $\phi$  can exceed 1.

In conclusion, our findings reveal that the particle shell, responsible for the high mobility of liquid marbles, is also the origin of their static friction. This rolling friction arises from the shear-induced yielding of the shell and is primarily governed by two parameters: the marble shape and the surface particle density. The shape determines the shear profile and the yielding region. Despite a quasi-spherical geometry, smaller marbles require larger tilt angles to initiate motion under gravity compared to larger, gravity-flattened marbles. This contrasts with their dynamic behavior, where smaller marbles roll faster [6, 26]. The particle surface density  $\phi$  controls the yield point via a logistic function, capturing the rheological behavior of the granular shell. Notably, yield begins to increase at the percolation threshold, with the inflection point of the logistic curve corresponding to the close-packing limit of the granular layer. However, the physical mechanism determining the steepness parameter  $\beta$  of the logistic

function in granular rafts remains an open question. Finally, our results underscore the critical role of surface particle fraction in maintaining low static friction, especially in applications where evaporation increases shell density over time. They also reveal the potential of liquid marbles as a model system to probe the rheology of granular rafts on curved interfaces.

*Acknowledgements*—We thank Dominic Vella for fruitful discussions. TM acknowledges the financial support provided by the Japan Society for the Promotion of Science (JSPS) - Grant-in-Aid for Scientific Research (B), 24K01341. SP acknowledges the financial support provided by JSPS KAKENHI Grant-in-Aid for Research Activity Start-up 24K22937. TM and PKR gratefully acknowledge the financial support provided by the JSPS Grant-in-Aid for JSPS Fellows 23KF0106. YT is grateful for the financial support from JST SPRING (Grant Number JPMJSP2108) and the Leadership Development Program for Ph.D. students at the University of Tokyo, School of Engineering.

\* These authors contributed equally to this work.

† poincloux@phys.aoyama.ac.jp

‡ mouterde@g.ecc.u-tokyo.ac.jp

- [1] Henri Lhuissier, Yoshiyuki Tagawa, Tuan Tran, and Chao Sun. Levitation of a drop over a moving surface. *Journal of Fluid Mechanics*, 733:R4, 2013.
- [2] Anaïs Gauthier, James C Bird, Christophe Clanet, and David Quéré. Aerodynamic leidenfrost effect. *Physical Review Fluids*, 1(8):084002, 2016.
- [3] Anne-Laure Biance, Christophe Clanet, and David Quéré. Leidenfrost drops. *Physics of fluids*, 15(6):1632–1637, 2003.
- [4] Satoshi Shibuichi, Tomohiro Onda, Naoki Satoh, and Kaoru Tsujii. Super water-repellent surfaces resulting from fractal structure. *The Journal of Physical Chemistry*, 100(50):19512–19517, 1996.
- [5] Ralf Blossey. Self-cleaning surfaces—virtual realities. *Nature materials*, 2(5):301–306, 2003.
- [6] Pascale Aussillous and David Quéré. Liquid marbles. *Nature*, 411(6840):924–927, 2001.
- [7] Maxime Paven, Hiroyuki Mayama, Takafumi Sekido, Hans-Jürgen Butt, Yoshinobu Nakamura, and Syuji Fujii. Light-driven delivery and release of materials using liquid marbles. *Advanced Functional Materials*, 26(19):3199–3206, 2016.
- [8] Yan Zhao, Jian Fang, Hongxia Wang, Xungai Wang, and Tong Lin. Magnetic liquid marbles: manipulation of liquid droplets using highly hydrophobic  $\text{Fe}_3\text{O}_4$  nanoparticles. *Advanced materials*, 22(6):707–710, 2010.
- [9] Pritam Kumar Roy, Yui Takai, Rui Matsubara, Mizuki Tenjimbayashi, and Timothée Mouterde. Hot liquid marbles. *Proceedings of the National Academy of Sciences*, 122(20):e2500619122, 2025.
- [10] Yifeng Sheng, Guanqing Sun, Jie Wu, Guanghui Ma, and To Ngai. Silica-based liquid marbles as microreactors.

- tors for the silver mirror reaction. *Angewandte Chemie*, 127(24):7118–7123, 2015.
- [11] Nuno M Oliveira, Rui L Reis, and João F Mano. The potential of liquid marbles for biomedical applications: a critical review. *Advanced healthcare materials*, 6(19):1700192, 2017.
- [12] Raja K Vadivelu, Harshad Kamble, Ahmed Munaz, and Nam-Trung Nguyen. Liquid marble as bioreactor for engineering three-dimensional toroid tissues. *Scientific reports*, 7(1):12388, 2017.
- [13] Hyobin Jeon, Keunhwan Park, Jeong-Yun Sun, and Ho-Young Kim. Particle-armored liquid robots. *Science Advances*, 11(12):eadt5888, 2025.
- [14] Junfei Tian, Tina Arbatan, Xu Li, and Wei Shen. Liquid marble for gas sensing. *Chemical Communications*, 46(26):4734–4736, 2010.
- [15] Xia Rong, Rammile Ettelaie, Sergey V Lishchuk, Huaigang Cheng, Ning Zhao, Fukui Xiao, Fangqin Cheng, and Hengquan Yang. Liquid marble-derived solid-liquid hybrid superparticles for co2 capture. *Nature communications*, 10(1):1854, 2019.
- [16] Agnes Pockels. Über randwinkel und ausbreitung von flüssigkeiten auf festen körpern. *Phys. Z*, 15:39–46, 1914.
- [17] C. G. L. Furmidge. Studies at phase interfaces. i. the sliding of liquid drops on solid surfaces and a theory for spray retention. *Journal of colloid science*, 17(4):309–324, 1962.
- [18] Panlin Jin, Kexin Zhao, Zoé Blin, Malou Allais, Timothée Mouterde, and David Quéré. When marbles challenge pearls. *The Journal of Chemical Physics*, 158(20):204709, 2023.
- [19] Pascale Aussillous and David Quéré. Properties of liquid marbles. *Proceedings of the Royal Society A: Mathematical, Physical and Engineering Sciences*, 462(2067):973–999, 2006.
- [20] Glen McHale and Michael I Newton. Liquid marbles: principles and applications. *Soft Matter*, 7(12):5473–5481, 2011.
- [21] Pietro Cicuta and Dominic Vella. Granular character of particle rafts. *Physical review letters*, 102(13):138302, 2009.
- [22] Suzie Protière. Particle rafts and armored droplets. *Annual Review of Fluid Mechanics*, 55(1):459–480, 2023.
- [23] Nicolaas P Kruyt and L Rothenburg. Shear strength, dilatancy, energy and dissipation in quasi-static deformation of granular materials. *Journal of Statistical Mechanics: Theory and Experiment*, 2006(07):P07021, 2006.
- [24] Bruno Andreotti, Yoël Forterre, and Olivier Pouliquen. *Granular media: between fluid and solid*. Cambridge University Press, 2013.
- [25] Guillaume Lagubeau, Antonella Rescaglio, and Francisco Melo. Armoring a droplet: Soft jamming of a dense granular interface. *Physical Review E*, 90(3):030201, 2014.
- [26] Lakshminarayanan Mahadevan and Yves Pomeau. Rolling droplets. *Physics of fluids*, 11(9):2449–2453, 1999.
- [27] Atul Varshney, A Sane, Shankar Ghosh, and S Bhat-tacharya. Amorphous to amorphous transition in particle rafts. *Physical Review E—Statistical, Nonlinear, and Soft Matter Physics*, 86(3):031402, 2012.
- [28] John Quintanilla, Salvatore Torquato, and Robert M Ziff. Efficient measurement of the percolation threshold for fully penetrable discs. *Journal of Physics A: Mathematical and General*, 33(42):L399, 2000.
- [29] László Fejes Tóth. *Regular figures*. Elsevier, 2014.
- [30] Dominic Vella, Pascale Aussillous, and L Mahadevan. Elasticity of an interfacial particle raft. *Europhysics Letters*, 68(2):212, 2004.
- [31] Etienne Jambon-Puillet, Christophe Josserand, and Suzie Protière. Wrinkles, folds, and plasticity in granular rafts. *Physical Review Materials*, 1(4):042601, 2017.
- [32] Suriya Prakash, Hugo Perrin, and Lorenzo Botto. Buckling of a monolayer of platelike particles trapped at a fluid-fluid interface. *Physical Review E*, 109(1):014801, 2024.

### End Matter

*Liquid marble preparation* — To form liquid marbles, we deposit with a micropipet a volume  $\Omega$  of water on a bed of lycopodium particles (Sigma Aldrich). The droplet is gently rolled until it appears covered with particles. The resulting liquid marble is then transferred to a small stainless steel Petri dish with a metal spoon. It is then rolled a few times to remove the excess of particles, and placed on the silicon wafer for static friction measurements.

*Experimental determination of the surface fraction* — The surface fraction  $\phi_o$  is determined by direct measurements from side view photographs. The liquid surface appears clearer than the particles, which, by taking a threshold of intensity, allows for the estimation of the surface fraction. We measured the surface fraction for liquid marbles with volumes  $\Omega = [2, 5, 7, 10, 30, 50, 100, 200 \text{ and } 300] \mu\text{L}$ , using four marbles per volume. We measured an average surface fraction of 83.0% with a standard deviation of 1.25%.

*Measurement of the marble surface area* — To estimate the change in surface fraction resulting from volume modification, we measure the surface area of liquid marbles using side-view images. Each image is binarized, and we identify the vertical axis of symmetry that divides the marble into two equal halves. Assuming the marble is a solid of revolution around this axis, we analyze one-half of the marble. We detect the edge of this half, which defines a planar curve  $\mathcal{C}$ . The full marble surface is then modeled as the surface of revolution generated by rotating  $\mathcal{C}$  around the axis of symmetry. We compute the arc length  $s$  of the curve  $\mathcal{C}$  and its centroid distance  $X$  from the axis. We finally compute the total surface area  $S = 2\pi sX$  using the first Pappus-Guldinus theorem.